with the calcium phosphate protocol supplied with the Stratagene Mammalian Transfection kit. Transfectants of both cell types were selected in the presence of G-418. Transfection of NIH 3T3 cells allowed assessment of the transforming activity of the constructs and the efficiency of the transfection procedure.
12. A 670-base pair Eco R1 fragment containing the coding sequences of H-*ras* was excised from plasmids pJCL30 and 33 [J. C. Lacal *et al.*, *Proc. Nat. Acad. Sci U.S.A.* **81**, 5305 (1984)] and cloned into pMEXneo. The ser^{186} mutation was generated by the Bio-Rad m13 in vitro mutagenesis kit.
13. J. H. Hancock, A. I. Magee, J. E. Childs, C. J. Marshall, *Cell* **57**, 1167 (1989).
14. pDM16 contains a cDNA of *trk* [D. Martin-Zanca, S. H. Hughes, M. Barbacid, *Nature* **319**, 743 (1986)]. pDM78 was obtained from D. Martin-Zanca (unpublished data) and contains an in vitro generated cDNA of the *trk5* allele [F. Coulier *et al.*, *Mol. Cell. Biol.* **10**, 4202 (1990)].
15. A. G. E. Pearse, *Histochemistry* (Little Brown, Boston, ed. 3, 1968), p. 697; A. Novikoff, P. M. Novikoff, O. M. Rosen, C. S. Rubin, *J. Cell Biol.* **87**, 180 (1980).
16. B. M. Spiegelman, M. Frank, H. Green *J. Biol. Chem.* **258**, 10083 (1983); A. B. Chapman, D. M. Knight, B. S. Dieckman, G. M. Ringold, *ibid.* **259**, 15548 (1984); J. D. Paulauskis and H. S. Sul, *ibid.* **263**, 7049 (1988); D. A. Bernlohr, C. W. Angus, M. D. Lane, M. A. Bolanowski, T. J. Kelly, *Proc. Natl. Acad. Sci. U.S.A.* **81**, 5468 (1984).
17. L. P. Kozak and E. H. Birkenmeier, *Proc. Natl. Acad. Sci. U.S.A.* **80**, 3020 (1983); J. S . Cook *et al.*, *ibid.* **85**, 2949 (1988); C. A. Amy *et al.*, *ibid.* **86**, 3114 (1989).
18. A. Toscani, D. R. Soprano, K. J. Soprano, *J. Biol. Chem.* **265**, 5722 (1990).
19. I. Guerrero, A. Pellicer, D. E. Burstein, *Biochem. Biophys. Res. Commun.* **150**, 1185 (1988).
20. B. M. T. Burgering, A. J. Snidjers, A. Maassen, A. J. van der Eb, J. L. Bos, *Mol. Cell. Biol.* **9**, 4312 (1989); A. Pintzas and D. A. Spandidos, *Gene Anal. Tech.* **6**, 125 (1989).
21. H. Cai, J. Szeberenky, G. M. Cooper, *Mol. Cell. Biol.* **10**, 5314 (1990); J. Szeberenky, H. Cai, G. M. Cooper, *ibid.*, p. 5324; Y. Ogiso *et al.*, *Cell Growth Differ.* **1**, 217 (1990).
22. T. Satoh, M. Endo, M. Nakafufu, S. Nakamura, Y. Kaziro, *Proc. Natl. Acad. Sci. U.S.A.* **87**, 5993 (1990); T. Satoh *et al.*, *ibid.*, p. 7926; J. B. Gibbs, M. S. Marshall, E. M. Scolnick, R. A. F. Dixon, U. S. Vogel, *J. Biol. Chem.* **265**, 20437 (1990).
23. We thank L. Kozak, M. D. Lane, D. Martin-Zanca, A. Pellicer, C. S. Rubin, S. Smith, B. M. Spiegelman, and K. J. Soprano for providing reagents, T. Bryan for technical support, C. Molloy for the protocol to estimate Ras·GTP complex, G. Englund for help with photography, and J. Silver and K. Peden for critically reading the manuscript. Supported in part by a sabbatical fellowship from the Ministerio de Educacion y Ciencia, Spain.

15 January 1991; accepted 24 April 1991

Visual Motion Commands for Pursuit Eye Movements in the Cerebellum

RICHARD J. KRAUZLIS* AND STEPHEN G. LISBERGER

Eye movements that follow a target (pursuit eye movements) facilitate high acuity visual perception of moving targets by transforming visual motion inputs into motor commands that match eye motion to target motion. The performance of pursuit eye movements requires the cerebellar flocculus, which processes both visual motion and oculomotor signals. Electrophysiological recordings from floccular Purkinje cells have allowed the identification of their firing patterns during generation of the image velocity and image acceleration signals used for pursuit. Analysis with a method based on a behavioral model converted the time-varying spike trains of floccular Purkinje cells into a description of the firing rate contributed by three visual motion signals and one oculomotor input. The flocculus encodes all the signals needed to guide pursuit.

MANY PRIMATE BEHAVIORS ARE guided by vision. Although much is known about the sensory processing of visual inputs, little is known about the sensory-motor transformations that convert central visual signals into commands for voluntary movements. Pursuit eye movements provide an opportunity to understand this sensory-motor transformation. Pursuit allows primates to use visual inputs related to image motion, defined as target motion with respect to the eye, to drive smooth eye movements that keep the eyes pointed at small moving targets. Previous experiments have led to the delineation of the brain areas that process moving images and the basic anatomical pathways that connect visual motion areas in the extrastriate cortex to the extraocular nuclei (*1*). In addition, our laboratory has developed a quantitative description of how visual motion signals are transformed to generate eye velocity (*2*). The next step is to determine how those signals are represented in the pursuit pathways.

Our experiments focus on the cerebellar flocculus, which is necessary for accurate pursuit (*3*) and is located at the interface between the visual and oculomotor pathways that generate pursuit eye movements. Visual inputs to the flocculus arise from at least the pontine nuclei and the nucleus reticularis tegmenti pontis, whereas inputs related to eye movements arise from the vestibular nuclei and the nucleus prepositus (*4*). Both the visual and oculomotor inputs are reflected in the simple-spike activity of floccular Purkinje cells (P cells), the output neurons of the cerebellum (*5*). In turn, neural activity of floccular P cells causes smooth eye movements within 10 ms by inhibiting the vestibular interneurons in the brainstem that project directly to extraocular motoneurons (*6*).

Our goal was to go beyond the previous demonstration of visual simple-spike responses in floccular P cells and provide a description of how properties of the visual inputs are related to features of pursuit. The design of our experiments was based on behavioral studies in monkeys, which suggested that three different visual signals provide the commands for smooth eye acceleration (*2*, 7). These signals are related to image velocity, the abrupt onset of image motion (image motion transient), and smooth changes in image velocity (image acceleration). Models of pursuit that include a sensitivity to all three visual signals have emergent properties that replicate several distinctive features of pursuit (*8*).

Figure 1 illustrates three target motions that can help dissect the visual inputs for pursuit into its three separate components. When the target is initially stationary and begins to move at a constant speed (Fig. 1A), all three components are available to contribute to pursuit. The image motion transient component, defined as the first derivative of image velocity for abrupt changes in target motion, makes a momentary contribution at the onset of target motion. The image velocity component provides an initial steady input that decreases toward zero as eye velocity increases toward target velocity. The image acceleration component, defined as the first derivative of image velocity for smooth changes in target motion, contributes after image velocity begins to decrease; this component acts in the direction opposite that of image velocity, braking eye velocity as it approaches the target velocity. When the target appears on the screen already moving (Fig. 1B), the image motion transient component does not contribute, and as a result the rising phase of eye velocity is less brisk. This target motion provides image velocity and image acceleration inputs that are qualitatively similar to those in Fig. 1A. When a target starts from rest and accelerates smoothly to a steady target velocity (Fig. 1C), the image velocity and image acceleration pathways contribute synergistically, and the image motion transient is not activated. The accelerating target

Department of Physiology, W. M. Keck Foundation Center for Integrative Neurosciences, and Neuroscience Graduate Program, University of California, San Francisco, CA 94143.

*To whom correspondence should be addressed.

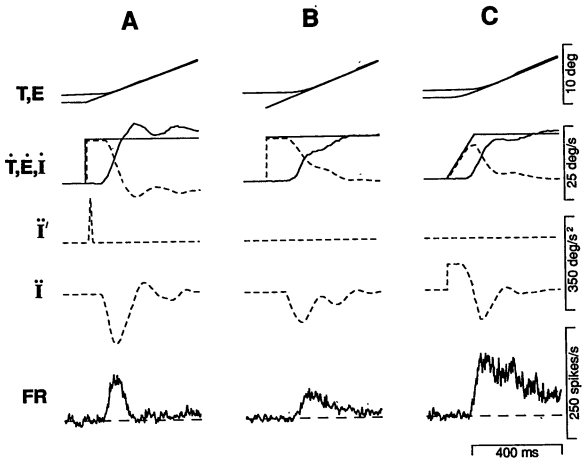

Fig. 1. Target motions used to dissociate visual motion and oculomotor signals used for pursuit. Each column shows one type of target motion. The different target motions produced different combinations of eye velocity and three visual motion signals. T and E are target and eye position; Ṫ, Ė, and İ are target, eye, and image velocity; T̈′ is image motion transient; T̈ is image acceleration; FR is P cell firing rate. In each case, the monkey initially fixated a central spot (not shown) until an eccentric target (0.5° white spot) began to move. (**A**) The target was visible and stationary for 300 to 500 ms at an eccentric position before it moved at a constant velocity. This variation of the step-ramp paradigm introduced by Rashbass (*16*) produces all three signals contained in our behavioral model: image velocity, an image motion transient, and image acceleration. (**B**) The target moved at a constant velocity but was not visible before the onset of its motion. The temporal coincidence of the target's appearance and its motion eliminates the motion transient signal present in (A). (**C**) The target accelerated smoothly from rest before achieving a constant velocity. The bottom row in each column shows the average firing rate recorded from a single P cell while a monkey performed these trials. The dashed line indicates the baseline firing rate of 90 spikes per second. These trials are samples from a set of target motions that consisted of constant velocity (5, 10, 20, and 30 deg/s) and accelerating targets (45, 80, 120, and 180 deg/s^2) moving in both the preferred and the nonpreferred directions. Measured variables (firing rate, target and eye position, and velocity) are shown as solid lines, whereas derived variables (image velocity, image motion transient, and image acceleration) are shown as dashed lines.

causes eye velocity to increase more briskly than would be predicted by the contribution of the image velocity pathway alone (7).

We recorded the simple-spike firing rate of single floccular P cells as monkeys with their heads restrained tracked constant velocity and smoothly accelerating targets such as those depicted in Fig. 1 (*9*). Inspection of the firing rate of the P cells during tracking of different target motions revealed that the firing pattern depended critically on which target motion was tracked. For example, the P cell in the bottom row of Fig. 1 showed a modest and sustained response when a target that moved at a constant velocity of 5 deg/s appeared (Fig. 1B). The same cell showed a larger and briefer response when a target moving at the same velocity started from rest (Fig. 1A) and a large and sustained response when the target accelerated smoothly at 180 deg/s^2 (Fig. 1C). The differences in firing rate reflect the differences in the visual and oculomotor signals associated with each target motion. However, the contribution of each input to the activity of the P cell could not be measured simply from the firing rate recorded during tracking of each target motion, because the visual motion and eye velocity signals varied con-

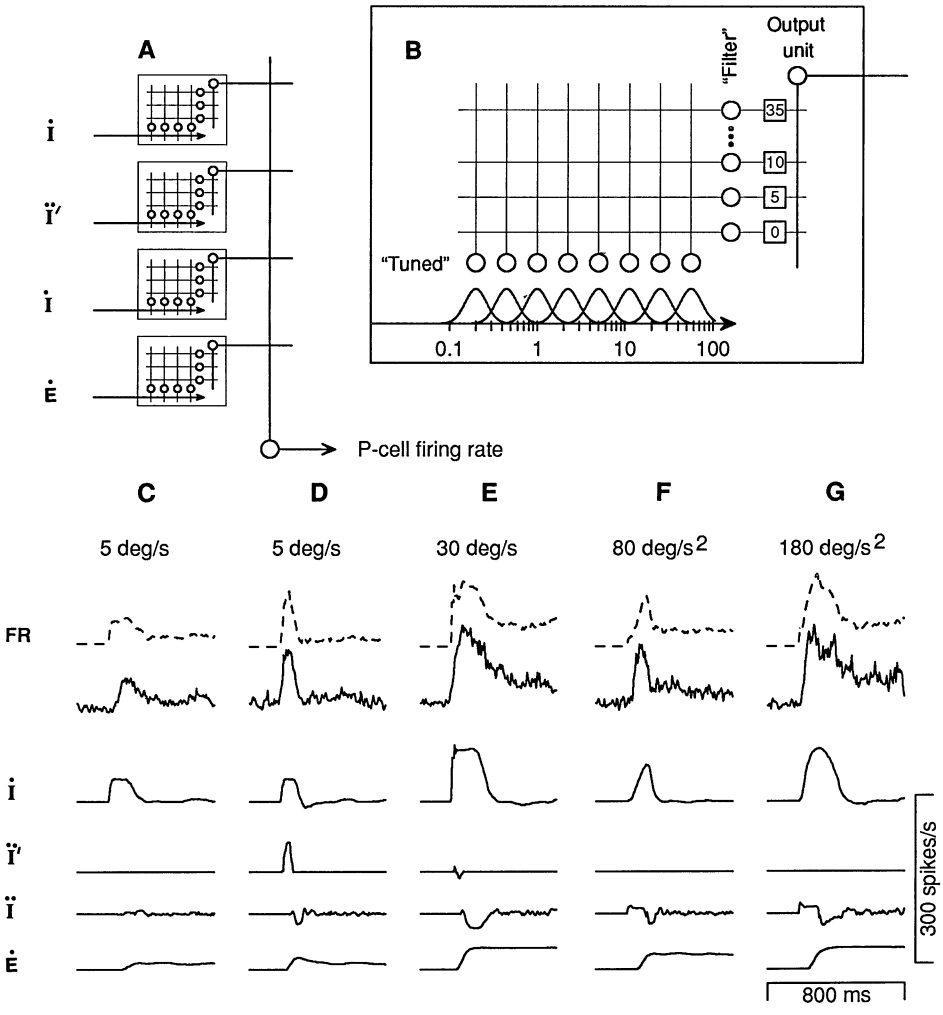

Fig. 2. (**A**) Distributed network model used to analyze P cell data. (**B**) Enlarged view of one network. Input signals activated tuned units (horizontal row of circles) that had log-Gaussian input-output functions. The Gaussian curves under the tuned units show how the output of each unit was related to input amplitude. Each network contained 16 tuned units, eight for positive and eight (not shown) for negative values of the input signal. Peaks of tuned units were located at fixed intervals on a log scale. The axis had units of either degrees per second or degrees per second squared, depending on the network. Peaks of extreme tuned units were located at 60 deg/s for image velocity, image motion transient, and eye velocity, and 500 deg/s^2 for image acceleration. The output of each filter unit (vertical row of circles) was delayed by a different amount of time (0 to 35 ms, indicated in boxes) and projected to a single output unit in the network. The three visual signal inputs were each delayed by 65 ms to account for the temporal offset in the contribution of visual motion inputs. (**C** through **G**) Sample fit of model to P cell firing rate profile. Traces are offset for clarity. The bottom four traces show the activity of output units in each of the four networks before being summed at the final unit. (C) shows the firing rate obtained during pursuit of a 5 deg/s target motion with no motion transient signal, like the target motion shown in Fig. 1B. (D) and (E) show firing rates obtained during pursuit of targets moving at 5 and 30 deg/s with a motion transient signal, as shown in Fig. 1A. (F) and (G) show firing rates for targets accelerating at 80 and 180 deg/s^2, like those shown in Fig. 1C. The SEs of the estimate provided by the model when compared to the firing rates shown in (C) through (G) were 7.876, 7.267, 7.602, 7.582, and 9.572, respectively. Much of this error is due to noise caused by the irregularity of P cell firing rate.

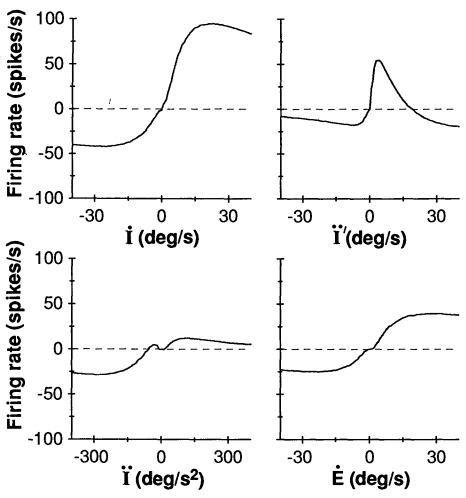

Fig. 3. Graphs relating firing rate to the amplitude of each input signal for the same P cell shown in Fig. 2.

tinuously as a function of time. It was therefore necessary to convert the time-varying averages of firing rate into a format that directly described the contribution of each input. We accomplished this transformation by first fitting the firing rate of each P cell with a separate copy of a model based on our behavioral analysis and then analyzing the properties of the models with the best fit.

The model used for data analysis consisted of four networks, each of which processed one input: image velocity, image motion transient, image acceleration, or eye velocity (Fig. 2A). The outputs of the four networks were summed to produce a simulated P cell firing rate. Each network consisted of interconnected units within a structure designed so that gradient descent adjustment of the weights (*10*) assigned to each connection could optimize how the input signals were scaled and filtered (Fig. 2B). Each "tuned" unit was activated by a different range of input values and produced an output that was a Gaussian function of its input. Filter units had different delays in their output lines. Adjusting the weights of the connections between tuned units and filter units allowed the model to customize the relation between the amplitude of each input signal and P cell firing rate. Adjusting the connections between filter units and the output unit of each network allowed the model to modify the temporal shape of each signal (*11*). The top two rows of traces in Fig. 2, C through G, show that the output of the optimized model (dashed lines) (*12*) was similar to the actual firing rate for a selection of target motions from one P cell (solid lines). Similar fits were obtained with the other 35 P cells in our sample (*13*).

The bottom four rows of traces in Fig. 2, C through G, show one example of how the model used the four input signals to account for P cell firing rate. The traces represent the activity of the output units from the four networks as a function of time and reveal the relative contribution of each input signal. For this P cell the output from the image velocity network contributed much of the response during tracking of each target motion. The network for the image motion transient accounted for the different responses to target motions with (Fig. 2, D and E) and without (Fig. 2C) a motion transient. The image acceleration signal made a large positive contribution to the model's output for smoothly accelerating targets (Fig. 2, F and G) and had a small inhibitory effect on the response to constant velocity targets (Fig. 2, D and E). As in the behavioral data in Fig. 1, this inhibitory effect was delayed and slowed the firing rate. Once tracking was accurate and image velocity and acceleration were small, most of the steady-state output of the model was attributed to eye velocity.

We next determined the signal processing attributed to each P cell by analyzing the four networks separately to obtain graphs relating firing rate to the amplitude of each input signal. For example, the four graphs in Fig. 3 represent the nonlinear transformations performed by the four networks used to fit the P cell firing rate in Fig. 2, C through G. We obtained the function plotted in each graph by providing input steps of different amplitudes to one of the four networks and measuring the activity of the output unit from that network 400 ms after the onset of the step. The model that provided the best fit to the firing rate of this P cell showed large saturating responses to image velocity and eye velocity, a large tuned response to the motion transient, and a more modest saturating response to image acceleration (*14*).

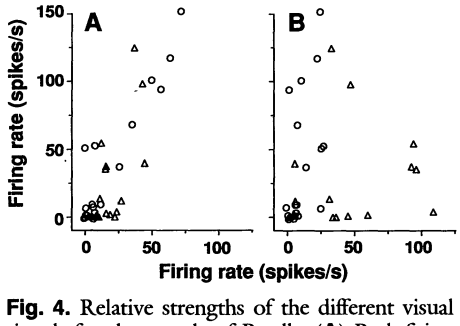

Fig. 4. Relative strengths of the different visual signals for the sample of P cells. (**A**) Peak firing rate due to the motion transient signal plotted as a function of that due to the image acceleration signal. (**B**) Modulation due to the motion transient signal plotted as a function of that due to the image velocity signal. Circles and triangles represent data from two different monkeys. The cells in the two monkeys showed a similar distribution of visual motion inputs except that the P cells with a very high sensitivity to image velocity were sampled only in one monkey.

Figure 4 shows the relative strengths of the different visual signals in our sample of P cells from two monkeys. For each P cell we measured the peak excitatory change in firing rate attributed to the three visual signals from graphs like those in Fig. 3. The broad distribution of response amplitudes shown in Fig. 4 indicates that the three visual motion signals were represented as a continuum in the population of P cells. In addition, plotting the peak firing rate attributed to the motion transient against that due to image acceleration revealed that P cells sensitive to one also tended to be sensitive to the other (Fig. 4A). However, there was no obvious relation between the peak firing rate due to the motion transient and that due to image velocity (Fig. 4B). These results suggest that the image acceleration and image motion transient signals represent a single component of the visual processing for pursuit, whereas velocity signals represent a separate component.

Our analysis of P cell firing describes how the cerebellar flocculus converts visual motion signals into commands for pursuit eye movements. It accounts for P cell firing under natural conditions in which the monkey generates pursuit eye velocity and sensory feedback is changing continuously. The model we used in our analysis is not the only way to fit the neural data, but the model's basis in behavioral observations on pursuit eye movements provides an appropriate starting point for localizing the neural representation of the signals used for pursuit. Our success in fitting the firing rate of floccular P cells with the same class of model that accounts for the details of pursuit eye velocity demonstrates that the output of the flocculus encodes all of the visual motion and oculomotor signals needed for pursuit.

The identification of functionally defined signals in floccular P cells is a first step toward quantifying the transformations accomplished by the neural substrates for pursuit. Because the anatomical pathways for pursuit are part of a corticopontocerebellar projection system that is important for the generation of many other movements (*15*), study of the sensory motor processing underlying pursuit eye movements is likely to provide insights into the neural control of more complex visually guided behaviors.

REFERENCES AND NOTES

1. For a review of pursuit eye movements, see S. G. Lisberger, E. J. Morris, and L. Tychsen [*Annu. Rev. Neurosci.* **10**, 97 (1987)].
2. R. J. Krauzlis and S. G. Lisberger, *Neural Comp.* **1**, 116 (1989).
3. D. S. Zee, A. Yamazaki, P. H. Butler, G. J. Gucer, *J. Neurophysiol.* **46**, 878 (1981).
4. P. Brodal, *J. Comp. Neurol.* **204**, 44 (1982); T.

Langer, A. F. Fuchs, C. A. Scudder, M. C. Chubb, *ibid.* **235**, 1 (1985).
5. S. G. Lisberger and A. F. Fuch, *J. Neurophysiol.* **41**, 733 (1978); F. A. Miles and J. H. Fuller, *Science* **189**, 1000 (1975); _____, D. J. Braitman, B. M. Dow, *J. Neurophysiol.* **43**, 1437 (1980); H. Noda and D. A. Suzuki, *J. Physiol.* (*London*) **294**, 349 (1979); L. S. Stone and S. G. Lisberger, *J. Neurophysiol.* **63**, 1241 (1990). Most recordings in primate "flocculus," including those reported here, have been made in the rostral folia, which recent anatomical data have shown are more accurately referred to as part of the ventral paraflocculus [N. M. Gerrits and J. Voogd, *Exp. Brain Res. Suppl.* **17**, 26 (1989)].
6. C. D. Balaban, M. Ito, E. Watanabe, *Neurosci. Lett.* **27**, 101 (1981); T. Langer, A. F. Fuchs, M. C. Chubb, C. A. Scudder, S. G. Lisberger, *J. Comp. Neurol.* **235**, 26 (1985); S. G. Lisberger and T. A. Pavelko, *Science* **242**, 771 (1988).
7. R. J. Krauzlis and S. G. Lisberger, *Soc. Neurosci. Abst.* **13**, 170 (1987).
8. Including a sensitivity to image acceleration allows the model to replicate the high-frequency oscillations often observed in pursuit eye velocity [E. J. Morris and S. G. Lisberger, *ibid.* **11**, 79 (1985); (*2*)], and also allows the model to account for the observation that the frequency of spontaneous oscillations during steady-state pursuit decreases when additional delays are imposed in visual feedback [D. Goldreich and S. G. Lisberger, *ibid.* **13**, 170 (1987); R. J. Krauzlis and S. G. Lisberger, *ibid.* **14**, 798 (1988); D. Goldreich, R. J. Krauzlis, S. G. Lisberger, *J. Neurophysiol.*, in press].
9. Detailed methods have been described by L. S. Stone and S. G. Lisberger in (*5*).
10. The gradient descent algorithm was based on the method of B. A. Pearlmutter [*Neural Comp.* **1**, 263 (1989)].
11. Adjusting the output weights of the filter units allowed the model to construct a finite impulse response filter. The weights were constrained to be nonnegative to prevent the network from differentiating the input signals (for example, converting eye velocity into eye acceleration). Time delays were constrained to be positive to prevent noncausal behavior of the analysis.
12. The difference between the output of the model and the traces of the averaged firing rate asymptotically reached a minimum after 500 to 1000 iterations of the gradient descent algorithm.
13. The average SE of the modeled fit for all 18 target motions with this P cell was 9.188. For the population of 36 P cells, the average SE ranged from 4.520 to 23.365 (mean ± SD = 12.166 ± 4.220). The model was normally optimized with data obtained from tracking all of the target motions described in Fig. 1. Training the model on a subset of the target motions produced nearly identical results but required more iterations. For most P cells, eliminating one or more networks from the model prevented the analysis from obtaining good fits to data from all trials.
14. The dead zones or inflections seen near the origin of some of these graphs were a common feature of our data. The reduced or reversed sensitivity to small-amplitude inputs could provide a way to achieve both rapid corrections in eye speed when target speed is changing and stable tracking when target speed is constant. The different response to small amounts of visual motion could be due to an indirect effect on simple-spike firing rate by climbing fiber inputs, which inhibit simple-spikes and have the opposite directional selectivity [L. S. Stone and S. G. Lisberger, *J. Neurophysiol.* **63**, 1262 (1990); *Exp. Brain Res. Suppl.* **17**, 299 (1989)].
15. P. Brodal, *Brain* **101**, 251 (1978); *Neuroscience* **4**, 193 (1979); M. Glickstein *et al.*, *J. Comp. Neurol.* **190**, 209 (1980).
16. C. Rashbass, *J. Physiol.* (*London*) **159**, 326 (1961).
17. Supported by NSF grant BNS8616509 and by a University of California Chancellor's Fellowship to R.J.K. Purchase of the computers used for the network model was made possible by Defense Advanced Research Projects Agency grant N00014-89-5-3094.

6 March 1991; accepted 17 May 1991